

Fully Spiking Neural Network for Legged Robots

Xiaoyang Jiang^{1,*}, Qiang Zhang^{2,*}, Jingkai Sun², Jiahang Cao², Jingtong Ma¹, Renjing Xu^{2,†}

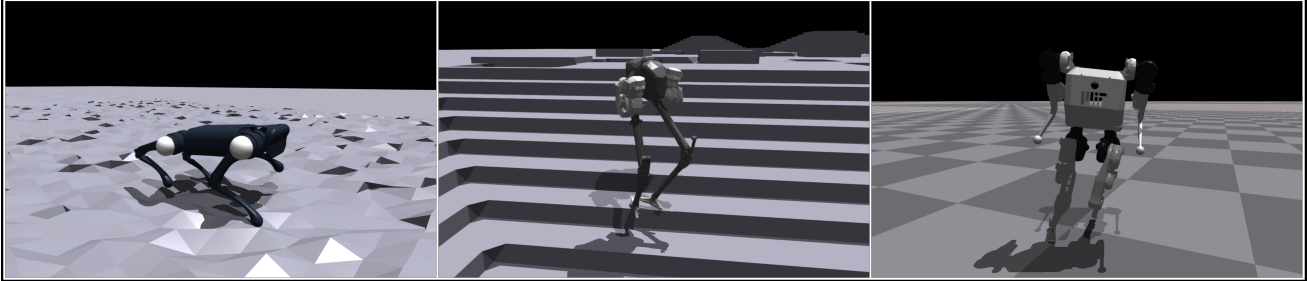


Fig. 1: Whole-body control on various types of robots through our spike-based approach. This innovative methodology allows us to effectively regulate and coordinate the robots' movements, enhancing their overall performance and versatility. **Left:** A1 **Middle:** Cassie **Right:** MIT Humanoid

Abstract—In recent years, legged robots based on deep reinforcement learning have made remarkable progress. Quadruped robots have demonstrated the ability to complete challenging tasks in complex environments and have been deployed in real-world scenarios to assist humans. Simultaneously, bipedal and humanoid robots have achieved breakthroughs in various demanding tasks. Current reinforcement learning methods can utilize diverse robot bodies and historical information to perform actions. However, prior research has not emphasized the speed and energy consumption of network inference, as well as the biological significance of the neural networks themselves. Most of the networks employed are traditional artificial neural networks that utilize multilayer perceptrons (MLP). In this paper, we successfully apply a novel Spiking Neural Network (SNN) to process legged robots, achieving outstanding results across a range of simulated terrains. SNN holds a natural advantage over traditional neural networks in terms of inference speed and energy consumption, and their pulse-form processing of body perception signals offers improved biological interpretability. Applying more biomimetic neural networks to legged robots can further reduce the heat dissipation and structural burden caused by the high power consumption of neural networks. To the best of our knowledge, this is the first work to implement SNN in legged robots.

I. INTRODUCTION

The increasing adoption of mobile robots, which are equipped with continuous high-dimensional observations and action space, to tackle a wide range of intricate tasks in real-world situations emphasizes the critical importance of exceptional control algorithms. Currently, the limited on-board energy resources of most robots pose a significant challenge, as this constraint hinders their ability to operate continuously and cost-effectively. Consequently, there is an immediate demand for developing energy-efficient solutions

for the seamless control of these autonomous machines. Deep reinforcement learning (DRL) employs deep neural networks (DNNs) as potent function approximators for learning optimal control strategies for intricate tasks [1], [2], through directly mapping the original state space to the action space [3], [4]. Nonetheless, the remarkable performance of DRL frequently comes at the expense of substantial energy consumption and slower execution speeds, making them unsuitable for various applications. Additionally, the execution speed of control strategies employing DNNs tends to be slower in comparison to the operational speed of the motion units. This discrepancy often results in a step-like behavior in the control signals, causing negative impacts on the performance of the system. Moreover, the reliance of current Deep Neural Networks (DNNs) on high-power GPUs for computation significantly impacts the structural design of robots, necessitating the inclusion of substantial active cooling systems.

Spiking neural networks (SNNs), also referred to as third-generation neural networks, present a promising alternative for energy-efficient and high-speed deep networks. These emerging SNNs operate based on the principles of neuromorphic computing, wherein the integration of memory and computation is seamless, and neurons engage in asynchronous, event-based communication and computation [5]. The biological plausibility, the significant increase in energy efficiency (particularly when deployed on neuromorphic chips [6]), high-speed processing and real-time capability for high-dimensional data (especially from asynchronous sensors like event-based cameras [7]) contribute to the advantages that SNNs possess over ANNs in specific applications. These advantages render the utilization of SNNs not only feasible but also highly advantageous in lieu of ANNs for performing effective calculations. A mounting body of research illustrates that SNNs can function as energy-efficient and high-speed solutions for effectively managing robot control in scenarios where there are limitations on onboard energy

*equal contributors, †the corresponding author (renjingxu@hkust-gz.edu.cn)

¹The authors are with Faculty of Robot Science and Engineering, Northeastern University, China

²The authors are with The Hong Kong University of Science and Technology (Guangzhou), China

resources [8]–[10]. To address the limitations of SNNs in tackling high-dimensional control problems, a natural approach involves combining the energy efficiency of SNNs with the optimality of DRL, which has proven effective in various control tasks [11]. Due to the role of rewards as training guides in reinforcement learning (RL), some studies utilize a three-factor learning rule [12] to implement reward learning. Although these rules exhibit strong performance in low-dimensional tasks, they often struggle to handle complex problems, and the optimization process becomes challenging in the absence of a global loss function [13]. Recently, [14] proposed a strategy gradient-based algorithm to train an SNN for learning random strategies. However, this algorithm is designed for discrete action spaces, and its practical applications are somewhat limited when tackling high-dimensional continuous control problems.

The recent conceptualization of the brain’s topology and computational principles has ignited advancements in SNNs, exhibiting both human-like behavior [15] and superior performance [16]. A pivotal attribute associated with effective computation in the brain is the employment of neuronal populations for encoding and representing information, encompassing the entire spectrum from sensory input to output signals. In this scenario, each neuron within a population has a receptive field that captures a specific segment of the encoded signal [17]. Notably, initial investigations into this group coding scheme have shown its enhanced capability to represent stimuli [18], contributing to recent triumphs in training SNNs for complex, high-dimensional supervised learning tasks [19], [20]. The efficacy of population coding presents a promising pathway for the advancement of efficient SNNs that leverage population coding. These networks possess the potential to acquire optimal solutions for complex high-dimensional continuous control tasks, paving the way for significant progress in this field.

The main contributions of this paper can be summarized as follows:

- For the first time, we have implemented SNNs on a policy network in various legged robots simulated in Isaac Gym [21], enabling the encoding of each dimension of the observation and action space within a single population of neurons using a learnable acceptance domain. Furthermore, we have successfully integrated this method and achieved successful training outcomes using techniques such as imitation learning and trajectory history.
- Our approach presents a considerable advantage over conventional ANNs in terms of energy efficiency. This advantage holds substantial significance for enhancing the structural integrity and reducing the costs associated with robot development.
- The research affirms the exceptional performance demonstrated by SNNs in the domain of high-frequency robot control, coupled with their significant edge over ANNs in attenuating signal noise, which enhances their robustness in practical situations.

II. RELATED WORK

A. Reinforcement Learning for Legged Robotics Locomotion

In recent years, there has been a rapid development of reinforcement learning techniques in the realm of achieving fast, stable, and adaptive locomotion for legged robots. [22] bridges the gap between reinforcement learning simulation and actual reality by modeling the actuator through neural networks. [23] utilizes the teacher-student training framework to integrate environmental parameters with preconceptions which enables quadruped robots to adapt to complex terrains. [24] introduces a large number of auxiliary rewards and gait parameter control to implement multiple gaits for a single policy. This work brings a lot of inspiration to the design of quadruped rewards. [25] combines reinforcement learning with computer vision to complete simultaneous locomotion and manipulation. Unlike traditional reinforcement learning, Generative adversarial imitation learning (GAIL) is an approach for imitating behaviors from reference datasets by integrating a generative adversarial network. Based on the GAIL, Adversarial Motion Priors (AMP) [26] combines the task reward and imitation reward to make the agent complete the tasks based on the action being similar to the reference dataset. For learning unlabeled references dataset, [27] uses a skill discriminator additionally and enables quadruped to distinguish and master multiple gaits, and perform backflips not found in the dataset. [28] combines RMA and AMP, allowing the quadruped with the ability to traverse challenging terrains rapidly. However, the above methods are realized by ANNs. Therefore, it cannot take into account the high-frequency and energy-saving advantages of SNNs.

B. Spiking Neuron Networks

Recently, many works have grown up around introducing SNNs into RL algorithms [12], [29]–[32]. SNNs offer advantages in processing temporal information, energy efficiency, event-driven processing, robustness to noise, plasticity, and biological plausibility. Some methods get trained ANNs to be converted into corresponding SNNs with few accuracy loss by matching the firing rates of spiking neurons with the graded activation of analog neurons [33].

Yet following the surrogate gradient method [34], the spike-based backpropagation (BP) algorithm has quickly become the mainstream solution for training multi-layer SNNs [35]. As shown in several open-source frameworks of SNNs [36], [37], the membrane voltage of non-spiking neurons is feasible to represent a continuous value in a spike-based BP method.

III. SNNs BASED LOCOMOTION IN ISAACGYM

We opted to evaluate the efficacy of our algorithm by training and testing it using Isaac Gym [21]. Isaac Gym is a simulation platform specifically created for robotics applications. The software provides a realistic physics simulation, specialized support for legged robots, integration with NVIDIA technologies, customizable features, and a vibrant community.

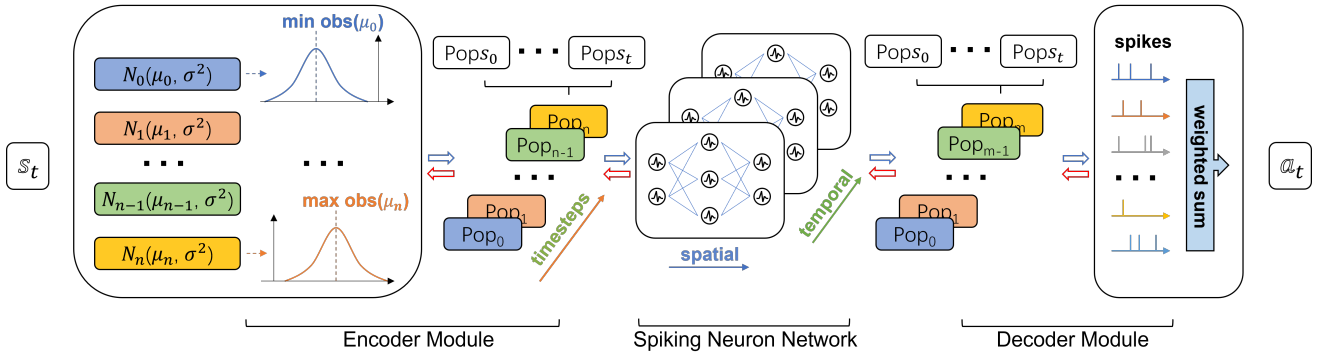


Fig. 2: The observations are initially encoded by the encoder as n independent distributions that are uniformly distributed over the observation range. After encoding, the population processes the distributions, resulting in spike generation. The neurons in the input populations encode each observation dimension and drive a multi-layered, fully connected SNN. During forward timesteps in PopSAN, the activities of each output population are decoded to determine the corresponding action dimension. This implies that the neural network receives observations, processes them using the SNN, and decodes the resulting activities to determine the appropriate action for the specific situation.

Algorithm 1 Forward propagation through PopSAN

Randomly initialize weight matrices \mathbf{W} and biases \mathbf{b} for each SNN layer;
Initialize encoding means μ and standard deviations σ for all input populations;
Randomly initialize decoding weight vectors \mathbf{W}_d and bias b_d for each action dimension;
 N -dimensional observation, \mathbf{s} ;
Spikes from input populations generated by encoder module: $\mathbf{X} = \text{Encoder}(\mathbf{s}, \mu, \sigma)$;
for $t = 1, \dots, T$ **do**
 Spikes at timestep t : $\mathbf{o}^{(t)(0)} = \mathbf{X}^{(t)}$;
 for $k = 1, \dots, K$ **do**
 Update LIF neurons in layer k at timestep t based on spikes from layer $k - 1$:
 $\mathbf{c}^{(t)(k)} = d_c \cdot \mathbf{c}^{(t-1)(k)} + \mathbf{W}^{(k)} \mathbf{o}^{(t)(k-1)} + \mathbf{b}^{(k)}$;
 $\mathbf{v}^{(t)(k)} = d_v \cdot \mathbf{v}^{(t-1)(k)} \cdot (1 - \mathbf{o}^{(t-1)(k)}) + \mathbf{c}^{(t)(k)}$;
 $\mathbf{o}^{(t)(k)} = \text{Threshold}(\mathbf{v}^{(t)(k)})$;
 end for
 end for
 M -dimensional action \mathbf{a} generated by decoder module:
 Sum up the spikes of output populations: $\mathbf{sc} = \sum_{t=1}^T \mathbf{o}^{(t)(K)}$;
 for $i = 1, \dots, M$ **do**
 Compute firing rates of the i^{th} output population:
 $\mathbf{fr}^{(i)} = \mathbf{sc}^{(i)}/T$;
 Compute i^{th} dimension of action: $\alpha^i = \mathbf{W}_d^{(i)} \cdot \mathbf{fr}^{(i)} + b_d^{(i)}$;
 end for

A. SNN based Policy Network

We employ a population-coded spiking actor-network (PopSAN) [38] that is trained in tandem with a deep critic network using the DRL algorithms (including RMA and AMP). During training, the PopSAN generated an action $\alpha \in \mathbb{R}^N$ for a given observation, \mathbf{s} , and the deep critic network predicted the associated state value $V(\mathbf{s})$ or action-value $Q(\mathbf{s}, \alpha)$, which in turn optimized the PopSAN, in accordance with a chosen DRL method (Fig. 2). Within the PopSAN architecture, the encoder module is responsible

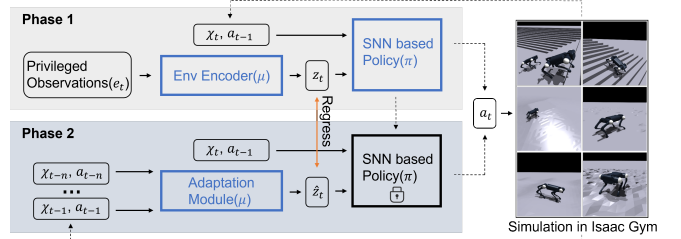


Fig. 3: RMA consists of two subsystems: the base policy π and the adaptation module ϕ . The RMA training consists of two phases. **Training the Base Policy (Phase 1)**: In the initial phase, the base policy π is trained using PopSAN. The system takes the current state x_t , the previous action a_{t-1} , and the environmental factors e_t as input. These environmental factors are encoded into a latent extrinsics vector z_t using the environmental factor encoder μ . **Training the Adaptation Module (Phase 2)**: In the second phase, the adaptation module ϕ is trained to predict the extrinsics \hat{z}_t using past states and actions. This training utilizes supervised learning with on-policy data. The adaptation module learns to capture the relationship between the state-action history and the corresponding extrinsics. By training the base policy and the adaptation module in these two phases, RMA can learn and adapt to the environment more effectively.

for encoding individual dimensions of the observation by mapping them to the activity of distinct neuron populations. During forward propagation, the input populations activate a multi-layer fully-connected SNN. The SNN then produces activity patterns within the output populations. At the end of each set of T timesteps, these patterns of activity are decoded in order to ascertain the associated action dimensions. (as outlined in Algorithm 1).

The current-based leaky-integrate-and-fire (LIF) model of a spiking neuron is employed in constructing the SNN. This model is utilized in constructing the SNN architecture. The dynamics of the LIF neurons are governed by a two-step model, as elaborated in Algorithm 1: i) the integration of presynaptic spikes o into current c ; and ii) the integration of current c into membrane voltage v ; d_c and d_v represent the current and voltage decay factors, respectively. In this particular implementation, a neuron fires a spike when its membrane potential surpasses a predetermined threshold. The hard-reset model was implemented, in which the membrane potential is promptly reset to the resting potential following a spike. The resultant spikes are transmitted to the post-synaptic neurons during the same inference timestep, under the assumption of zero propagation delay. This approach facilitates efficient and synchronized information transmission within the SNN.

Next, we combined the advantages of SNN with the advanced RMA algorithm. Figure 3 shows that the RMA system consists of two interconnected subsystems: the base policy π and the adaptation module ϕ . These subsystems work together to support continuous adaptation in various environmental conditions, ensuring seamless online operations. The base policy is trained using reinforcement learning in simulation, leveraging privileged information about the environment configuration e_t , such as friction, payload, and other factors. By utilizing the vector e_t , the base policy can adapt effectively to the unique characteristics of the environment.

Unfortunately, implementing this policy directly is not feasible in reality because e_t is unavailable. To address this challenge, we must estimate the extrinsics during runtime, a task performed by the adaptation module ϕ . The actual movement of robot joints deviates from the intended movement due to extrinsic influences. Instead of depending on privileged information, we can use the agent’s recent state history to estimate the extrinsics vector. The purpose of ϕ is to estimate the extrinsics vector z_t based solely on the recent state and action history of the robot, without direct access to e_t .

In addition, we have successfully combined SNN with AMP and achieved similar performance to ANN on legged robots. Figure 4 provides a schematic overview of the system. The motion dataset M consists of a collection of reference motions, where each motion $m^i = \hat{q}_t^i$ is represented as a sequence of poses \hat{q}_t^i . The motion clips can be obtained from a variety of sources, including motion capture (mocap) recordings of real-life actors or artist-authored keyframe animations. The simulated robot’s movement is governed by a policy $\pi(\alpha_t|s_t, g)$ that links the character’s state s_t and a given goal g to a distribution of actions α_t . The policy generates actions that determine the desired target positions for proportional-derivative (PD) controllers at each joint of the robot. The controllers then generate control forces to propel the robot’s motion according to specified target positions. The goal g defines a task reward function $r_t^G = r^G(s_t, \alpha_t, s_{t+1}, g)$ that outlines the high-level objectives the robot needs to achieve. The style objective $r_t^S = r^S(s_t, s_{t+1})$ is determined by an adversarial discriminator, which provides an a priori estimate of the naturalness or style of a motion, independent of the task at hand. By doing this, the style objective encourages the policy to produce movements that closely mirror the behaviors seen in the dataset.

B. Training of Legged Robot using SNN on Isaacgym

In our study, we used gradient descent to update the PopSAN parameters, with the specific loss function depending on the algorithm chosen (RMA or AMP). To train PopSAN parameters, we use the gradient of the loss with respect to the computed action, denoted as $\nabla_a L$. The parameters for each output population $i, i \in 1, \dots, M$ are updated independently as follows:

$$\nabla_{\mathbf{W}_d^{(i)}} L = \nabla_{\alpha_i} L \cdot \mathbf{W}_d^{(i)} \cdot \mathbf{f} \mathbf{r}^{(i)}, \nabla_{b_d^{(i)}} L = \nabla_{\alpha_i} L \cdot \mathbf{W}_d^{(i)} \quad (1)$$

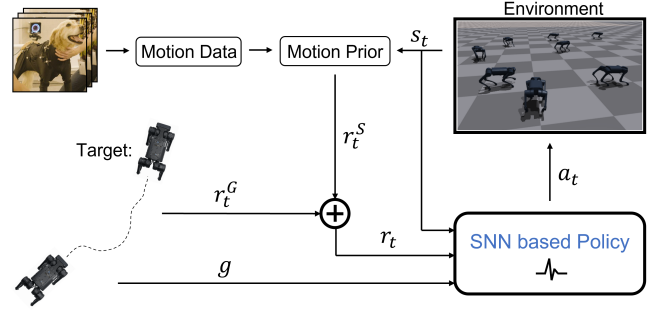


Fig. 4: By leveraging Adversarial Motion Priors and employing PopSAN as a replacement for the policy network during training, the agent is able to generate behaviors that capture the essence of the motion capture dataset.

The SNN parameters are updated using extended spatiotemporal backpropagation as introduced in [39]. We utilized the rectangular function $z(v)$, as defined in [40], to estimate the spike’s gradient. The gradients of the loss with respect to the parameters of the SNN for each layer k are computed by aggregating the gradients backpropagated from all timesteps:

$$\nabla_{\mathbf{W}^{(k)}} L = \sum_{t=1}^T \mathbf{o}^{(t)(k-1)} \cdot \nabla_{\mathbf{c}^{(t)(k)}} L, \nabla_{\mathbf{b}^{(k)}} L = \sum_{t=1}^T \nabla_{\mathbf{c}^{(t)(k)}} L \quad (2)$$

Lastly, we updated the parameters independently for each input population $i, i \in 1, \dots, N$ as follows:

$$\begin{aligned} \nabla_{\mu^{(i)}} L &= \sum_{t=1}^T \nabla_{\mathbf{o}_i^{(t)(o)}} L \cdot \mathbf{A}_E^{(i)} \cdot \frac{s_i - \mu^{(i)}}{\sigma^{(i)^2}}, \\ \nabla_{\sigma^{(i)}} L &= \sum_{t=1}^T \nabla_{\mathbf{o}_i^{(t)(o)}} L \cdot \mathbf{A}_E^{(i)} \cdot \frac{(s_i - \mu^{(i)})^2}{\sigma^{(i)^3}} \end{aligned} \quad (3)$$

IV. EXPERIMENTS

The objectives of our experiments are the followings: i) To validate the feasibility of SNNs on robots operating in environments with high latitudes and intricate dynamics models. ii) Verify the benefits of SNNs over ANNs in terms of ultra-high flatness control. iii) Identify rewards that SNNs excel on rl tasks and make improvements on poorly performing rewards. We assessed our approach using the Isaac Gym platform, which offers precise physics simulation and a versatile, customizable framework for robot models and environments.

We primarily evaluated the performance of the following robots: A1, Cassie [41], and MIT Humanoid [42] where each SNN is trained within 1,500,000 iterations until convergence. The ultimate assessment involves utilizing visual representations and metrics, including base linear velocity in the x and y axes, angular velocity in the yaw axis, mean episode length, and position torque are used for evaluation.

A. Simulation Setup

In order to establish a varied array of environments, we incorporated multiple URDF files from recent studies. The files contain various models, including A1, Anymal-b, Anymal-c, Cassie, MIT Humanoid, and others. Once imported, we utilize the functionalities of the Isaac Gym

TABLE I: Ranges of the environmental parameters

Parameters	Training range	Testing range
Friction	[0.005, 4.5]	[0.004, 6.0]
K_p	[50, 60]	[45, 65]
K_d	[0.4, 0.8]	[0.3, 0.9]
Payload(Kg)	[0, 6]	[0, 7]
Center of Mass(cm)	[-0.15, 0.15]	[-0.18, 0.18]
Motor Strength	[0.90, 1.10]	[0.88, 1.22]
Re-sample Probability	0.004	0.01

simulator to generate novel environments for each of these models. To introduce diversity, we make use of the built-in fractal terrain generator offered by the simulator. This terrain generator facilitates the creation of diverse types of terrain, encompassing flat terrains as well as rugged terrains with a variety of topographical characteristics. The policy functions at a control frequency of up to 500Hz, attributed to our SNN-based approach. This capability enables the attainment of high-frequency control, leading to prompt and precise adjustments to the system. In Table I listed a comprehensive list of environmental variations and their respective ranges is presented.

B. Performances of High Frequency Control using SNNs

We conducted tests on the robots mentioned above specifically for linear and angular velocity tracking tasks. In these tests, we considered tracking velocity (linear and angular) as the primary positive rewards. Additionally, we incorporated penalties for base height that is too low, excessive acceleration, and instances where the robot falls, etc. For A1, we conducted training and testing in several terrain environments, including pyramid stairs like terraces (upstairs and downstairs), pyramids with sloping surfaces, hilly terrains, terrains with discrete obstacles, and terrains covered with stepping stones. On the other hand, Cassie is solely trained in a trapezoidal pyramid environment and MIT Humanoid in a plain terrain.

1) *A1*: To explore the benefits of SNNs in high-frequency control scenarios, we intentionally increased the simulation environment’s time step (dt) to 2.5 times the default ANNs task, achieving a frequency of 500Hz. Our goal is to determine if SNN outperforms ANN in real-world environments that demand high-frequency control by comparing their performance.

The investigation is motivated by the limitations robots face when using ANN control algorithms due to energy constraints. As a result, these robots can typically only achieve a policy inference frequency of 100Hz, significantly lagging behind the motors’ execution frequency. Instead, SNN has the potential to improve policy inference quality and provide real-time control performance by leveraging its energy-efficient nature and deployment on specialized processors. If SNN can match or outperform ANN in high-frequency control, it would demonstrate SNN’s superiority in real-world environments.

In Figure 5, the effectiveness of our method under high-frequency control is clearly demonstrated. The A1 robot

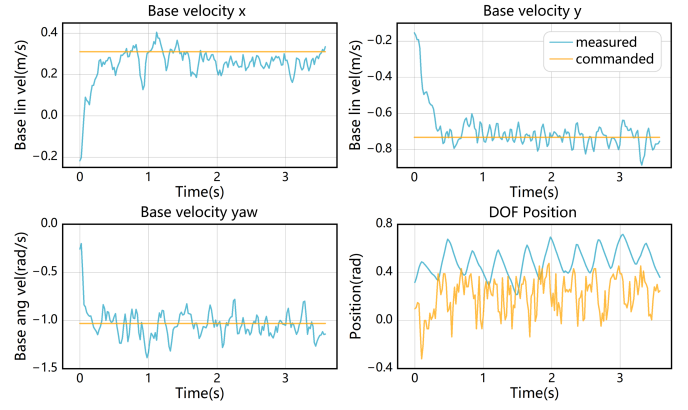


Fig. 5: The four graphs depicting the robot’s x-axis linear velocity, y-axis linear velocity, yaw-axis angular velocity, and DOF position vividly demonstrate the successful accomplishment of the task through the implementation of our method.

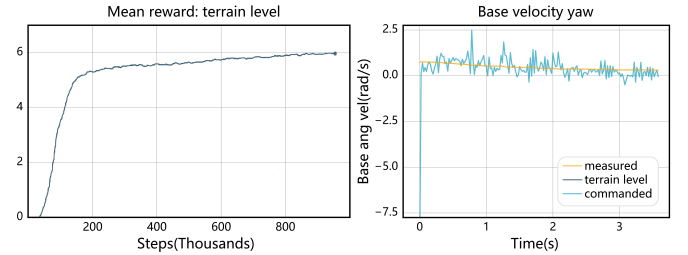


Fig. 6: The first image showcases Cassie’s remarkable capability to conquer complex terrain, as indicated by the terrain level value nearing 6. Additionally, the second figure demonstrates Cassie’s impeccable tracking of the angular velocity of the yaw axis, exemplifying its capacity to maintain body stability while traversing complex terrain.

demonstrates impressive performance in tracking velocity x , accurately following the desired trajectory. Considering the impact of complex terrain conditions, all velocities varied within a margin of 17% around the designated value. Although occasional spikes occur, indicating moments when the robot deviates from the existing policy framework, these instances can be attributed to the robot’s inclination to explore alternative approaches when faced with challenging terrain. This emphasizes the robustness of our method in tackling challenging terrains.

2) *Cassie*: In Cassie’s experiments, a trapezoidal pyramid environment was utilized, with terrain level indicates the absolute value of the robot’s elevation displacement (a value of 6 signifies reaching the top of the sixth-order pyramid). The training results of the Cassie robot have proven to be highly successful, as shown in Figure 6. The stability of the angular velocity along the yaw axis is notable. This stability is crucial for maintaining effective control and balance while navigating diverse terrains. Furthermore, the robot’s impressive ability to reach the highest terrain levels demonstrates its adaptability in conquering rugged landscapes. These findings highlight the Cassie robot’s ability to navigate difficult terrains effectively using SNNs at a high control frequency while maintaining stability. Consequently, the feasibility of our approach is confirmed, supporting its potential deployment in complex and dynamic real-world scenarios.

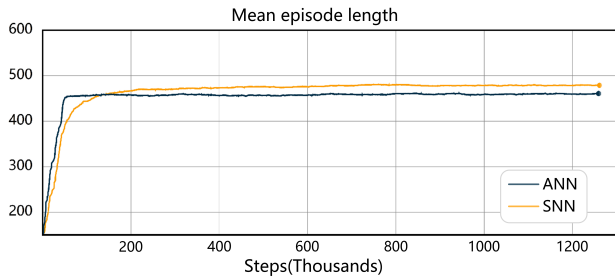


Fig. 7: In experiments conducted on the MIT Humanoid, the SNN achieves a comparable level of approximation with ANN in multiple evaluation metrics and even surpasses ANN. Despite the fact that SNN takes longer to train, the SNN outperforms ANN in terms of mean episode length after training convergence, providing strong evidence for the exceptional robustness of our method in whole body control.

3) *MIT Humanoid*: The training of MIT Humanoid also proved to be highly successful, showcasing the effectiveness of our spike-based approach. While it did take slightly longer to train compared to the traditional ANNs, the results obtained are equally impressive. In fact, they even surpassed the ANN in certain individual metrics, as clearly depicted in Figure 7. These findings strongly suggest that the SNN possesses inherent advantages when it comes to control robustness. Furthermore, it enables agents to not only thrive but also endure in their environment for an extended duration. This highlights the potential of SNN as a powerful tool in enhancing agent performance and longevity.

The performance demonstrated by our approach, whether through AI and Cassie’s agile traversal of challenging terrains or the MIT Humanoid’s unrestricted running, is undeniably superior.

C. Continuity Comparison

Compared to ANN, SNN also shows stronger robustness. This is because in SNNs the signaling relies on thresholding, leading to the direct exclusion of some noise. The stochastic behavior of spiking neuron dynamics also enhances the robustness of the network to external noise. We added Gaussian noise to the robot’s movement commands, and tested the performance of the networks with two strategies, ANN and SNN, for sigma of 0.1, 0.2, and 0.3, respectively, using the following of the robot’s y-axis linear velocity as an index. The experiment (Figure 8) proves that as the noise increases, the SNN’s ability to resist noise becomes more and more obvious, and its measurements become closer to the desired value and are accompanied by less fluctuations. On the other hand, the situation of ANN is not optimistic, at sigma of 0.3, the trained strategy is completely insufficient to support the robot to walk normally, and falls occurred. Under the same noise interference, the robot with SNN as the policy network can still walk smoothly.

D. Estimation of Energy Consumption

As mentioned earlier, one of the primary advantages of our SNN policy is its minimal energy usage. The assessment of energy consumption in a SNN is complex because the floating-point operations (FLOPs) in the initial encoder layer are MAC, whereas all other Conv or FC layers are AC. Building upon prior research [43]–[46] conducted by SNN,

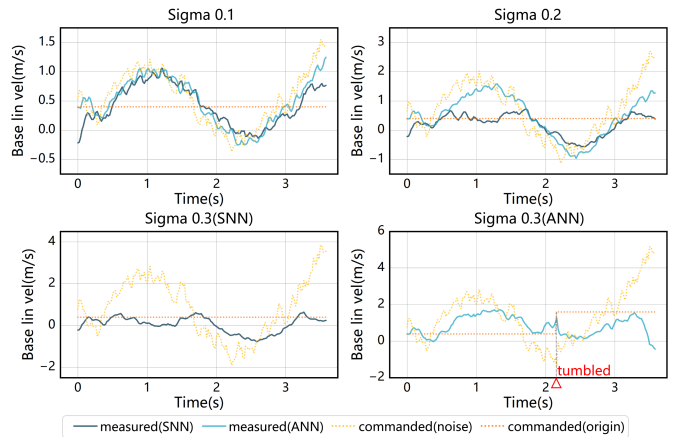


Fig. 8: Linear velocity following case. The original command was set to 0.4, and Gaussian noise with a scaling factor of 0.1 was introduced. SNN consistently surpasses that of ANN when subjected to equivalent levels of noise, with this difference widening as the noise level intensifies. At a sigma of 0.3 for Gaussian noise, the robot with SNN as its strategy maintained stable command following and smooth walking, whereas the ANN version of the robot experienced instability and tumbled.

TABLE II: Energy Comparison ($\times 10^{-6}$ mJ)

Method	Actor(T=1)	Actor(T=2)	Actor(T=3)
ANN Model	85.96	85.96	85.96
SNN Model(ours)	3.35	15.36	35.22
Energy Saving	96.10%	82.13%	59.03%

it is assumed that the data utilized for various operations is represented in 32-bit floating-point format in 45nm technology [45], with $E_{MAC} = 4.6\text{pJ}$ and $E_{AC} = 0.9\text{pJ}$. The energy consumption equations simulated for SNN are provided as follows:

$$E_{model} = E_{MAC} \cdot FL_{SNNConv}^1 + E_{AC} \cdot \left(\sum_{n=2}^N FL_{SNNConv}^n + \sum_{m=1}^M FL_{SNNFC}^m \right) \quad (4)$$

Experimental results (Table II) demonstrate that our approach offers a significant energy efficiency improvement compared to the conventional ANN architecture. Specifically, it achieves energy savings of 95.65%, 81.49%, and 60.34% at T = 1, 2 and 3, respectively.

V. CONCLUSION

This study presents the integration of SNN with history trajectory and imitation learning, which achieves performance comparable to ANNs, highlights the versatility of SNNs in policy gradient-based DRL algorithms. This opens up new horizons for application of SNNs in various reinforcement learning tasks, including continuous control.

Additionally, our approach offers significant advantages in energy efficiency, addressing signal noise, and high-frequency control. These advantages are significant for improving structural integrity and robustness in practical situations. It also has potential to reduce costs related to robot development and enables the implementation of advanced sensing systems in robotic platforms.

By embracing SNNs, we unlock a realm of possibilities for future advancements in intelligent control systems, transcending traditional computational paradigms.

REFERENCES

- [1] S. Ha, J. Kim, and K. Yamane, "Automated deep reinforcement learning environment for hardware of a modular legged robot," in *2018 15th international conference on ubiquitous robots (UR)*. IEEE, 2018, pp. 348–354.
- [2] Y. Zhu, R. Mottaghi, E. Kolve, J. J. Lim, A. Gupta, L. Fei-Fei, and A. Farhadi, "Target-driven visual navigation in indoor scenes using deep reinforcement learning," in *2017 IEEE international conference on robotics and automation (ICRA)*. IEEE, 2017, pp. 3357–3364.
- [3] Y. Duan, X. Chen, R. Houthoofd, J. Schulman, and P. Abbeel, "Benchmarking deep reinforcement learning for continuous control," in *International conference on machine learning*. PMLR, 2016, pp. 1329–1338.
- [4] T. P. Lillicrap, J. J. Hunt, A. Pritzel, N. Heess, T. Erez, Y. Tassa, D. Silver, and D. Wierstra, "Continuous control with deep reinforcement learning," *arXiv preprint arXiv:1509.02971*, 2015.
- [5] M. Davies, N. Srinivasa, T.-H. Lin, G. Chinya, Y. Cao, S. H. Choday, G. Dimou, P. Joshi, N. Imam, S. Jain *et al.*, "Loihi: A neuromorphic manycore processor with on-chip learning," *Ieee Micro*, vol. 38, no. 1, pp. 82–99, 2018.
- [6] K. Roy, A. Jaiswal, and P. Panda, "Towards spike-based machine intelligence with neuromorphic computing," *Nature*, vol. 575, no. 7784, pp. 607–617, 2019.
- [7] G. Gallego, T. Delbrück, G. Orchard, C. Bartolozzi, B. Tabak, A. Censi, S. Leutenegger, A. J. Davison, J. Conradt, K. Daniilidis *et al.*, "Event-based vision: A survey," *IEEE transactions on pattern analysis and machine intelligence*, vol. 44, no. 1, pp. 154–180, 2020.
- [8] G. Tang, A. Shah, and K. P. Michmizos, "Spiking neural network on neuromorphic hardware for energy-efficient unidimensional slam," in *2019 IEEE/RSJ International Conference on Intelligent Robots and Systems (IROS)*. IEEE, 2019, pp. 4176–4181.
- [9] T. Taunayazov, W. Sng, H. H. See, B. Lim, J. Kuan, A. F. Ansari, B. C. Tee, and H. Soh, "Event-driven visual-tactile sensing and learning for robots," *arXiv preprint arXiv:2009.07083*, 2020.
- [10] C. Michaelis, A. B. Lehr, and C. Tetzlaff, "Robust trajectory generation for robotic control on the neuromorphic research chip loihi," *Frontiers in neurobotics*, vol. 14, p. 589532, 2020.
- [11] V. Mnih, K. Kavukcuoglu, D. Silver, A. A. Rusu, J. Veness, M. G. Bellemare, A. Graves, M. Riedmiller, A. K. Fidjeland, G. Ostrovski *et al.*, "Human-level control through deep reinforcement learning," *nature*, vol. 518, no. 7540, pp. 529–533, 2015.
- [12] N. Frémaux, H. Sprekeler, and W. Gerstner, "Reinforcement learning using a continuous time actor-critic framework with spiking neurons," *PLoS computational biology*, vol. 9, no. 4, p. e1003024, 2013.
- [13] R. Legenstein, C. Naeger, and W. Maass, "What can a neuron learn with spike-timing-dependent plasticity?" *Neural computation*, vol. 17, no. 11, pp. 2337–2382, 2005.
- [14] B. Rosenfeld, O. Simeone, and B. Rajendran, "Learning first-to-spike policies for neuromorphic control using policy gradients," in *2019 IEEE 20th International Workshop on Signal Processing Advances in Wireless Communications (SPAWC)*. IEEE, 2019, pp. 1–5.
- [15] P. Balachandrar and K. P. Michmizos, "A spiking neural network emulating the structure of the oculomotor system requires no learning to control a biomimetic robotic head," in *2020 8th IEEE RAS/EMBS International Conference for Biomedical Robotics and Biomechatronics (BioRob)*. IEEE, 2020, pp. 1128–1133.
- [16] R. Kreiser, A. Renner, V. R. Leite, B. Serhan, C. Bartolozzi, A. Glover, and Y. Sandamirskaya, "An on-chip spiking neural network for estimation of the head pose of the icub robot," *Frontiers in Neuroscience*, vol. 14, p. 551, 2020.
- [17] A. P. Georgopoulos, A. B. Schwartz, and R. E. Kettner, "Neuronal population coding of movement direction," *Science*, vol. 233, no. 4771, pp. 1416–1419, 1986.
- [18] G. Tkačik, J. S. Prentice, V. Balasubramanian, and E. Schneidman, "Optimal population coding by noisy spiking neurons," *Proceedings of the National Academy of Sciences*, vol. 107, no. 32, pp. 14419–14424, 2010.
- [19] G. Bellec, D. Salaj, A. Subramoney, R. Legenstein, and W. Maass, "Long short-term memory and learning-to-learn in networks of spiking neurons," *Advances in neural information processing systems*, vol. 31, 2018.
- [20] Z. Pan, J. Wu, M. Zhang, H. Li, and Y. Chua, "Neural population coding for effective temporal classification," in *2019 International Joint Conference on Neural Networks (IJCNN)*. IEEE, 2019, pp. 1–8.
- [21] V. Makoviychuk, L. Wawrzyniak, Y. Guo, M. Lu, K. Storey, M. Macklin, D. Hoeller, N. Rudin, A. Allshire, A. Handa *et al.*, "Isaac gym: High performance gpu-based physics simulation for robot learning," *arXiv preprint arXiv:2108.10470*, 2021.
- [22] J. Hwangbo, J. Lee, A. Dosovitskiy, D. Bellicoso, V. Tsounis, V. Koltun, and M. Hutter, "Learning agile and dynamic motor skills for legged robots," *Science Robotics*, vol. 4, no. 26, p. eaa5872, 2019.
- [23] A. Kumar, Z. Fu, D. Pathak, and J. Malik, "Rma: Rapid motor adaptation for legged robots," *arXiv preprint arXiv:2107.04034*, 2021.
- [24] G. B. Margolis and P. Agrawal, "Walk these ways: Tuning robot control for generalization with multiplicity of behavior," in *Conference on Robot Learning*. PMLR, 2023, pp. 22–31.
- [25] Y. Ji, G. B. Margolis, and P. Agrawal, "Dribblebot: Dynamic legged manipulation in the wild," *arXiv preprint arXiv:2304.01159*, 2023.
- [26] X. B. Peng, Z. Ma, P. Abbeel, S. Levine, and A. Kanazawa, "Amp: Adversarial motion priors for stylized physics-based character control," *ACM Transactions on Graphics (ToG)*, vol. 40, no. 4, pp. 1–20, 2021.
- [27] C. Li, S. Blaes, P. Kolev, M. Vlastelica, J. Frey, and G. Martius, "Versatile skill control via self-supervised adversarial imitation of unlabeled mixed motions," in *2023 IEEE International Conference on Robotics and Automation (ICRA)*. IEEE, 2023, pp. 2944–2950.
- [28] J. Wu, G. Xin, C. Qi, and Y. Xue, "Learning robust and agile legged locomotion using adversarial motion priors," *IEEE Robotics and Automation Letters*, 2023.
- [29] R. V. Florian, "Reinforcement learning through modulation of spike-timing-dependent synaptic plasticity," *Neural computation*, vol. 19, no. 6, pp. 1468–1502, 2007.
- [30] M. J. O'Brien and N. Srinivasa, "A spiking neural model for stable reinforcement of synapses based on multiple distal rewards," *Neural Computation*, vol. 25, no. 1, pp. 123–156, 2013.
- [31] M. Yuan, X. Wu, R. Yan, and H. Tang, "Reinforcement learning in spiking neural networks with stochastic and deterministic synapses," *Neural computation*, vol. 31, no. 12, pp. 2368–2389, 2019.
- [32] K. Doya, "Reinforcement learning in continuous time and space," *Neural computation*, vol. 12, no. 1, pp. 219–245, 2000.
- [33] B. Rueckauer, I.-A. Lungu, Y. Hu, M. Pfeiffer, and S.-C. Liu, "Conversion of continuous-valued deep networks to efficient event-driven networks for image classification," *Frontiers in neuroscience*, vol. 11, p. 682, 2017.
- [34] J. H. Lee, T. Delbruck, and M. Pfeiffer, "Training deep spiking neural networks using backpropagation," *Frontiers in neuroscience*, vol. 10, p. 508, 2016.
- [35] W. Fang, Z. Yu, Y. Chen, T. Masquelier, T. Huang, and Y. Tian, "Incorporating learnable membrane time constant to enhance learning of spiking neural networks," in *Proceedings of the IEEE/CVF international conference on computer vision*, 2021, pp. 2661–2671.
- [36] W. Fang, Y. Wang, L. Pang, Z. Gu, Y. Wei, Y. Liu, P. Zhang, C. Chen, X. Zhou, Y. Liu *et al.*, "Lymph node metastasis in thymic malignancies: a chinese multicenter prospective observational study," *The Journal of Thoracic and Cardiovascular Surgery*, vol. 156, no. 2, pp. 824–833, 2018.
- [37] C. Pehle and J. E. Pedersen, "Norse—a deep learning library for spiking neural networks," *Version 0.0*, vol. 6, p. 25, 2021.
- [38] G. Tang, N. Kumar, R. Yoo, and K. Michmizos, "Deep reinforcement learning with population-coded spiking neural network for continuous control," in *Conference on Robot Learning*. PMLR, 2021, pp. 2016–2029.
- [39] G. Tang, N. Kumar, and K. P. Michmizos, "Reinforcement co-learning of deep and spiking neural networks for energy-efficient mapless navigation with neuromorphic hardware," in *2020 IEEE/RSJ International Conference on Intelligent Robots and Systems (IROS)*. IEEE, 2020, pp. 6090–6097.
- [40] Y. Wu, L. Deng, G. Li, J. Zhu, and L. Shi, "Spatio-temporal back-propagation for training high-performance spiking neural networks," *Frontiers in neuroscience*, vol. 12, p. 331, 2018.
- [41] N. Rudin, D. Hoeller, P. Reist, and M. Hutter, "Learning to walk in minutes using massively parallel deep reinforcement learning," in *Conference on Robot Learning*. PMLR, 2022, pp. 91–100.
- [42] S. H. Jeon, S. Heim, C. Khazoom, and S. Kim, "Benchmarking potential based rewards for learning humanoid locomotion," in *2023 IEEE International Conference on Robotics and Automation (ICRA)*. IEEE, 2023, pp. 9204–9210.
- [43] Y. Hu, Y. Wu, L. Deng, and G. Li, "Advancing residual learning

towards powerful deep spiking neural networks. arxiv," *preprint*]. doi, vol. 10, 2021.

- [44] S. Kundu, M. Pedram, and P. A. Beerel, "Hire-snn: Harnessing the inherent robustness of energy-efficient deep spiking neural networks by training with crafted input noise," in *Proceedings of the IEEE/CVF International Conference on Computer Vision*, 2021, pp. 5209–5218.
- [45] B. Yin, F. Corradi, and S. M. Bohté, "Accurate and efficient time-domain classification with adaptive spiking recurrent neural networks," *Nature Machine Intelligence*, vol. 3, no. 10, pp. 905–913, 2021.
- [46] M. Yao, G. Zhao, H. Zhang, Y. Hu, L. Deng, Y. Tian, B. Xu, and G. Li, "Attention spiking neural networks," *IEEE transactions on pattern analysis and machine intelligence*, 2023.